ADVANCED MATERIALS

www.advmat.de

Alumina-Supported CoFe Alloy Catalysts Derived from Layered-Double-Hydroxide Nanosheets for Efficient Photothermal CO_2 Hydrogenation to Hydrocarbons

*Guangbo Chen, Rui Gao, Yufei Zhao, Zhenhua Li, Geoffrey I. N. Waterhouse, Run Shi, Jiaqing Zhao, Mengtao Zhang, Lu Shang, Guiyang Sheng, Xiangping Zhang, Xiaodong Wen, Li-Zhu Wu, Chen-Ho Tung, and Tierui Zhang**

A series of novel CoFe-based catalysts are successfully fabricated by hydrogen reduction of CoFeAl layered-double-hydroxide (LDH) nanosheets at 300–700 °C. The chemical composition and morphology of the reaction products (denoted herein as CoFe-*x*) are highly dependent on the reduction temperature (*x*). CO_2 hydrogenation experiments are conducted on the CoFe-*x* catalysts under UV–vis excitation. With increasing LDH-nanosheet reduction temperature, the CoFe-*x* catalysts show a progressive selectivity shift from CO to CH_4, and eventually to high-value hydrocarbons (C_{2+}). CoFe-650 shows remarkable selectivity toward hydrocarbons (60% CH_4, 35% C_{2+}). X-ray absorption fine structure, high-resolution transmission electron microscopy, Mössbauer spectroscopy, and density functional theory calculations demonstrate that alumina-supported CoFe-alloy nanoparticles are responsible for the high selectivity of CoFe-650 for C_{2+} hydrocarbons, also allowing exploitation of photothermal effects. This study demonstrates a vibrant new catalyst platform for harnessing clean, abundant solar-energy to produce valuable chemicals and fuels from CO_2.

Anthropogenic CO_2 emissions caused by the combustion of fossil fuels for electricity generation and transportation are the primary cause of global warming. Conservative estimates suggest that global warming will increase mean global temperatures by as much as 3–4 °C over the next 50 years.[1] In an attempt to slow or minimize the environmental impacts of global warming, various approaches are currently being explored to curb CO_2 emissions, including more efficient use of fossil fuels and CO_2 capture and storage,[2] as well as chemical conversion of CO_2 into high-value chemicals and fuels.[3] The latter is a very desirable approach, though technically very demanding. Catalytic CO_2 hydrogenation represents arguably the most important and viable pathway for large-scale CO_2 utilization.[4] Catalysts

G. Chen, Dr. Y. Zhao, Z. Li, R. Shi, J. Zhao, Dr. L. Shang, Prof. L.-Z. Wu, Prof. C.-H. Tung, Prof. T. Zhang
Key Laboratory of Photochemical Conversion and Optoelectronic Materials
Technical Institute of Physics and Chemistry
Chinese Academy of Sciences
Beijing 100190, P. R. China
E-mail: tierui@mail.ipc.ac.cn

G. Chen, Z. Li, J. Zhao
Key Laboratory of Synthetic and Natural Functional Molecule Chemistry of the Ministry of Education
College of Chemistry and Materials Science
Northwest University
Xi'an 710127, P. R. China

G. Chen
Center for Advancing Electronics Dresden (Cfaed) & Department of Chemistry and Food Chemistry
Technische Universitaet Dresden
01062 Dresden, Germany

The ORCID identification number(s) for the author(s) of this article can be found under https://doi.org/10.1002/adma.201704663.

DOI: 10.1002/adma.201704663

Dr. R. Gao, Prof. X. Wen
State key Laboratory of Coal Conversion
Institute of Coal Chemistry
Chinese Academy of Sciences
Taiyuan 030001, P. R. China

Dr. R. Gao, Prof. X. Wen
Synfuels China
Beijing 100195, P. R. China

Prof. G. I. N. Waterhouse
School of Chemical Sciences
The University of Auckland
Auckland 1142, New Zealand

R. Shi, Prof. T. Zhang
University of Chinese Academy of Sciences
Beijing 100049, P. R. China

M. Zhang
College of Chemistry and Molecular Engineering
Peking University
Beijing 100871, P. R. China

G. Sheng, Prof. X. Zhang
Institute of Process Engineering
Chinese Academy of Sciences
Beijing 100190, P. R. China

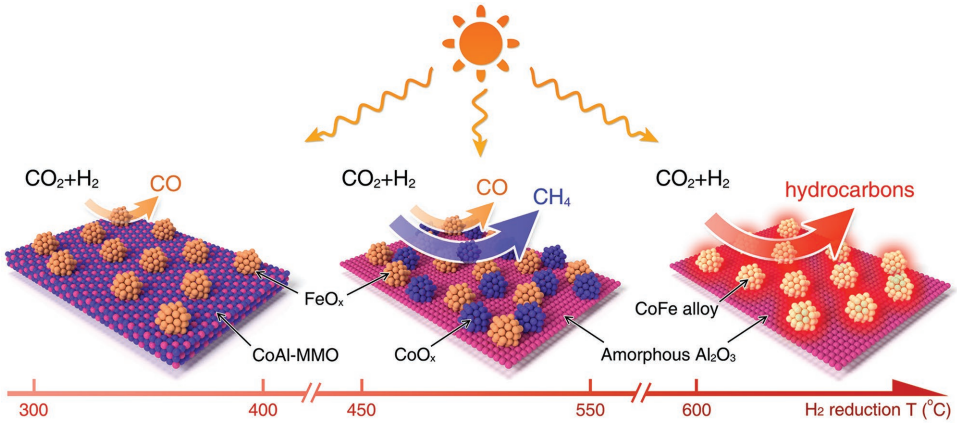

Scheme 1. Illustration of the different CoFe-*x* catalysts formed by hydrogen reduction of a CoFeAl-LDH nanosheet precursor at different temperatures. The CO_2 hydrogenation selectivity of each CoFe-*x* catalyst is indicated.

developed to date for CO_2 hydrogenation are typically based on supported Fe, Co, Ni or Ru (and their combinations), with product selectivity for CO_2 hydrogenation controlled by the unique electronic structure at catalytic active sites. Generally, monometallic Ni- and Ru-based catalysts mainly yield methane due to their strong hydrogenation ability.[5] Compared with Co, which tends to produce methane in CO_2 hydrogenation reaction,[6] Fe-based catalysts yield higher-value hydrocarbons (C_{2+}) due to their reverse water gas shift (RWGS) activity and Fischer–Tropsch synthesis (FTs) activity.[4d,7] Transformation of CO_2 to hydrocarbon fuels (light alkanes) has therefore great potential for both reducing CO_2 emissions and slowing our consumption of fossil-fuel reserves.

Although various Fe-based catalysts have been developed for CO_2 hydrogenation to hydrocarbons, most require harsh temperature and pressure conditions (e.g., 250–450 °C, 2–5 MPa) to achieve meaningful CO_2 conversions. The massive energy input required to drive CO_2 hydrogenation using such conventional thermal catalytic methods negates any benefits from carrying out the reaction.[8] Accordingly, alternative low-energy-input technologies need to be discovered for CO_2 hydrogenation, prompting a serious rethink of both catalyst design and operating mechanism. Compared with traditional thermal technologies, solar-driven CO_2 hydrogenation is a far more promising strategy, making use of abundant and clean solar energy.[9] In pursuit of this goal, considerable research effort is currently being directed toward the development of catalysts that can drive CO_2 hydrogenation under visible light. Recent pioneering research by Ye and co-workers demonstrated that group VIII nanocatalysts showed excellent photothermal catalytic performance for the hydrogenation of CO_2 to CH_4.[10] Other work by the same group showed that MOF-derived Fe@C core–shell nanostructures and Ru@layered double hydroxides (LDHs) hybrid catalysts afforded efficient visible light-induced CO_2 conversion to CO and CH_4, respectively.[11] Other catalysts such as Au–ZnO, Ru/Si nanowires, Pd@Nb_2O_5, Au&Pt@ZIF, and Ru/Al_2O_3 have also been reported to display good activities for photoinduced CO_2 hydrogenation.[12] Although these studies successfully demonstrate solar-driven CO_2 hydrogenation, the main products in all these systems are low-value-added C_1 compounds, CH_4 and CO (Table S1, Supporting Information). Tuning the reaction selectivity toward higher-value C_{2+} hydrocarbons such as ethane, propane, butane, or heavier alkanes is a priority, though this has proved enormously challenging. As mentioned above, single component Fe-based catalysts are active for the conversion of CO_2 to CO through RWGR ($CO_2 + H_2 \rightarrow CO + H_2O$), whilst Co is active for C—C coupling in the FTs (thereby offering pathways from $CO + H_2$ to C_{2+} hydrocarbons).[13] Therefore, synergistically combining metallic Fe and Co catalysts in the form of a CoFe alloy catalyst appeared a logical strategy for the development of novel solar-driven CO_2 hydrogenation catalysts with high selectivity toward valuable C_{2+} hydrocarbons. Recently, LDH structure has been regarded as the efficient catalyst precursors for the formation of highly dispersed metal supported catalysts for the further application.[14]

Herein, a series of novel CoFe-based catalysts (denoted CoFe-*x*) were fabricated by direct H_2 reduction of CoFeAl-LDH nanosheets at temperatures (*x*) between 300 and 700 °C, and their performance of CO_2 hydrogenation was systematically explored under simulated solar excitation. By increasing the reduction temperature of the LDH precursor from 300 to 700 °C, the surface chemistry of the CoFe-*x* catalysts could be precisely modified and the product selectivity of CO_2 hydrogenation was tuned progressively from CO to CH_4 and eventually high-value C_{2+} hydrocarbons (**Scheme 1**). Under UV–vis irradiation, the CoFe-650 catalyst showed a CO_2 conversion of 78.6%, with selectivity to C_{2+} of 35.26%. In addition to excellent catalytic activity under visible-light irradiation, the CoFe-650 catalyst demonstrated very good operational stability during cycling tests. Comprehensive catalyst characterization studies and density functional theory (DFT) calculations revealed that CoFe-650 catalyst consisted of alumina-supported CoFe alloy nanoparticles, with the formation of the discrete alloy nanoparticles underpinning the high C—C coupling selectivity. Photothermal effects caused by catalyst heating under UV–vis excitation contribute to the outstanding performance. To the best of our knowledge, this is the first study to report the synthesis of C_{2+} hydrocarbons in high yields via light-induced CO_2 hydrogenation.

Alumina-supported CoFe-containing catalysts were obtained by reducing CoFeAl-LDH nanosheets (Figure S1, Supporting Information) in an H_2/Ar (10/90, v/v) atmosphere at temperatures ranging from 200 to 700 °C. The obtained catalysts were denoted

as CoFe-*x* (where *x* is the reduction temperature). The H_2-reduction-induced topological transformation of the CoFeAl-LDH nanosheets was followed by X-ray diffraction (XRD) (Figure S2, Supporting Information). The analysis showed that the typical (*00l*) basal reflections of the LDH nanosheets disappeared with reduction temperatures above 200 °C, indicating the collapse of the LDH structure. LDH nanosheets reduction at temperatures between 300 and 550 °C yielded mixture of FeO_x and CoO_x nanoparticles supported on amorphous Al_2O_3 nanosheets. Reduction at 600 °C and above resulted in the formation of alumina-supported cubic CoFe alloy nanoparticles (JCPDS 48–1818).

Since the aim of this work was to develop solar-driven catalyst for CO_2 hydrogenation, the optical absorption properties of the CoFe-*x* catalysts warranted careful examination. As shown in Figure S3 of the Supporting Information, all CoFe-*x* catalysts prepared at temperatures above 200 °C showed intense light absorption across the ultraviolet to visible region. This strong light absorption by the CoFe-*x* catalysts contributed to their excellent performance for CO_2 hydrogenation, as discussed below. The activity of the CoFe-*x* catalysts (and selected reference catalysts including Co_3O_4, Fe_2O_3, Fe_3O_4, and mixtures of Fe_3O_4 and Co_3O_4) for CO_2 hydrogenation was evaluated under UV–vis light irradiation without any additional energy input (no external heating). The reaction gas mixture consisted of 0.18 MPa $CO_2/H_2/Ar$ = 15/60/25, with a reaction time of 2 h. The performance of the different catalysts is summarized in **Table 1**. A blank experiment conducted in the absence of catalyst or H_2 yielded no hydrocarbons or CO, demonstrating that both a catalyst and H_2 were indispensable for solar-driven CO_2 conversion. Upon light irradiation, the CoFeAl-LDH precursor and CoFe-200 exhibited no catalytic activity toward CO_2 conversion (Table 1, entries 2, 3). When the precursor reduction temperature was increased to 300 °C, the resulting CoFe-300 catalyst showed some activity for CO_2 conversion, with a 6% conversion mainly to CO (Table 1, entry 4). The CO_2 conversion gradually increased to 12.2% for CoFe-400, with high selectivity again to CO (Table 1, entry 5). Surprisingly, when the reduction temperature was increased 450 °C, a large amount of CH_4 (91.4% selectivity) was generated at reasonable CO_2 conversion (41.2%). However, CoFe-450 produced few C_{2+} hydrocarbons (C_{2+} selectivity ≈2.5%, Table 1, entry 6). This same high CH_4 selectivity and poor C_{2+} selectivity were also found for CoFe-500 and CoFe-550 (Table 1, entries 7, 8). Remarkably, when the LDH precursor reduction temperature was increased to 600 °C, the methane selectivity dropped to ≈60.0% and the selectivity to high-value C_{2+} hydrocarbons increased from ≈3.0% to 36.3% with 76.9% CO_2 conversion (Table 1, entry 9). Increasing the precursor reduction temperature to 650 and 700 °C caused only slight improvements in catalyst performance (Table 1, entries 10, 11). From the catalytic tests, CoFe-650 catalyst was selected for further investigation, with the aim of understanding its excellent catalytic performance for CO_2 hydrogenation to hydrocarbons, especially the C_{2+} product stream. As revealed in **Figure 1**a, the conversion of CO_2 increased with UV–vis irradiation time over the first 2 h of reaction, and then began to plateau as all the CO_2 in the reactor was almost consumed (reaching 86.5% CO_2 conversion after 3 h). The C_{2+} selectivity remained stable at ≈37.0% throughout the reaction without a photoinduced hydrogenolysis.[15] After irradiation for 2 h, the carbon product distribution followed an Anderson–Schulz–Flory distribution with a relatively small growth factor (α) of 0.345, indicating an FTs-like carbon chain growth mechanism (Figure 1b; Figure S4 and Table S2, Supporting Information). The aforementioned blank experiment, as well as isotope-tracing experiments (Figure S5, Supporting Information) using $^{13}CO_2$ conclusively demonstrated that the CH_4 and C_{2+} hydrocarbon products originated from the CO_2 feed mixture rather than surface absorbed carbon species on the catalysts. Results presented here thus conclusively demonstrate value-added hydrocarbons can be successfully synthesized by CO_2 hydrogenation over CoFe-650 under simulated solar excitation. Importantly, the selectivity to CO of this particular catalyst is very low (5.6%), with almost all the CO_2 feedstock being transformed into hydrocarbons.

Table 1. Performance comparison of CoFe-*x* and reference catalysts for the CO_2 hydrogenation under UV–vis excitation (unless otherwise stated).

Entry	Catalyst[a]	CO_2 conversion [%]	Product selectivity [%]			α[b]	C_{2+} (% C_xHy)[c]
			CO	CH_4	C_{2+}		
1	Blank[d]	0	–	–	–	–	–
2	CoFeAl-LDH	0	–	–	–	–	–
3	CoFe-200	0	–	–	–	–	–
4	CoFe-300	6.1	99.99	0.01	–	–	–
5	CoFe-400	12.2	99.99	0.01	–	–	–
6	CoFe-450	41.2	6.04	91.45	2.51	–	2.67
7	CoFe-500	56.8	6.56	91.21	2.23	–	2.38
8	CoFe-550	68.2	6.42	90.89	2.69	–	2.87
9	CoFe-600	76.9	5.19	58.49	36.32	0.318	38.31
10	CoFe-650	78.6	4.97	59.77	35.26	0.345	37.10
11	CoFe-700	79.9	5.53	60.08	34.39	0.334	36.40
12	CoFe-650[e]	44.8	5.03	60.16	34.81	0.341	36.65
13	CoFe-650[f]	82.2	2.97	60.61	36.42	0.342	37.53
14	Fe_2O_3[g]	16.6	100.00	–	–	–	–
15	Fe_3O_4[g]	19.5	100.00	–	–	–	–
16	Co_3O_4[g]	77.9	–	99.98	0.02	–	–
17	Co_3O_4 + Fe_3O_4[h]	41.2	5.07	92.34	2.59	–	2.73

[a]Reaction conditions: catalyst mass, 100 mg; $CO_2/H_2/Ar$ = 15/60/25; 0.18 MPa; irradiation time, 2 h; irradiation source, 300 W Xe light (UV–vis light), with no external heat input; [b]α refers to the growth factor of hydrocarbons; [c]C_{2+} selectivity in hydrocarbons; [d]Blank experiments, including irradiation in the absence of any catalyst, irradiation of the catalysts in Ar or pure CO_2 over CoFe-650 catalyst under above conditions; [e]Irradiation under visible light for 2 h; [f]Irradiation under UV–vis–IR light for 2 h; [g]Commercial available reference catalysts, details are in the Supporting Information; [h]Mixed reference catalyst, 67.0 mg Co_3O_4 and 33.0 mg Fe_3O_4.

In order to clarify the catalytic nature of CO_2 hydrogenation over CoFe-650 as light-induced photothermal catalysis or photocatalysis,[10,16] we conducted some experiments where we monitored the temperature of the catalysis bed using a thermocouple in intimate contact with the catalyst bed. As shown in Figure 1c, upon UV–vis irradiation the temperature of CoFe-650 catalyst increased rapidly over a period of around 20 min, stabilizing at 310 °C after 30 min. At such high temperatures, the catalytic

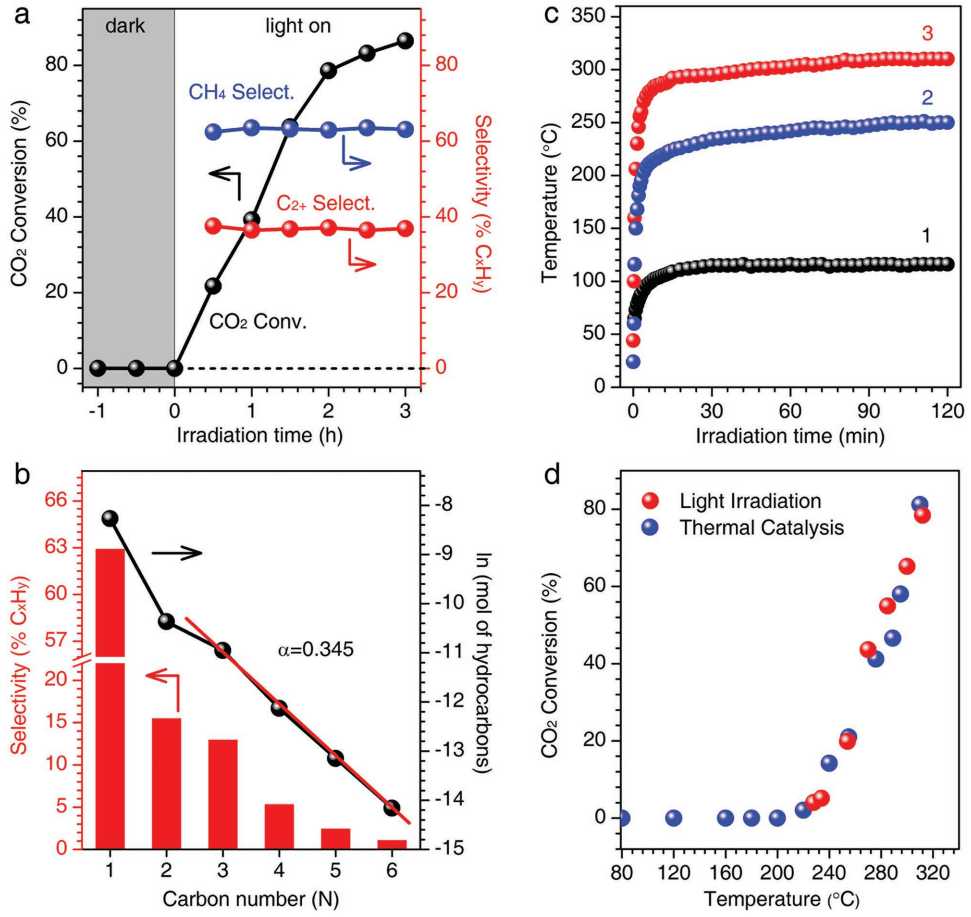

Figure 1. a) Time course of CO_2 conversion and product selectivities for CO_2 hydrogenation over CoFe-650 under UV–vis irradiation. b) The hydrocarbon product distribution obtained over CoFe-650 under UV–vis irradiation for 2 h. c) Temperature profiles for: (1) reactor without any catalyst under UV–vis irradiation, (2) CoFe-650 under visible irradiation, and (3) CoFe-650 upon UV–vis irradiation. d) Comparison of CO_2 conversion for CoFe-650 under photothermal heating (UV–vis irradiation) and direct thermal heating (no UV–vis irradiation).

CO_2 hydrogenation reaction was almost certainly photothermally driven. To gain further evidence to support the existence the photothermal CO_2 hydrogenation pathway, we examined the effect of UV–vis irradiation intensity on the surface temperature of the CoFe-650 catalyst (Figure S6, Supporting Information). A strong linear relationship was established. Perhaps the most convincing evidence for the photothermal pathway is seen in Figure 1d, where the conversion of CO_2 during CO_2 hydrogenation is plotted against reaction temperature for CoFe-650 under UV–vis irradiation (i.e., heating by UV–vis absorption) and under direct external heating (no UV–vis irradiation). The CO_2 conversion profiles are near identical with temperature. Accordingly, it can be concluded that CO_2 hydrogenation to valuable hydrocarbons over CoFe-650 almost certainly occurs *via* a photothermal pathway rather than a photocatalytic route. The production capacity of the catalysts is of great interest for practical applications, with results shown in Table S3 of the Supporting Information. In addition, the CoFe-650 catalyst also displayed excellent stability with the stable activity and C_{2+} selectivity over a number of test cycles (Figure S7, Supporting Information), with no obvious phase change detected by XRD (Figure S8, Supporting Information). Moreover, the CoFe-650 catalyst also showed the catalytic performance toward the generation of value-added compounds under visible-light irradiation (λ > 420 nm) and UV–vis–IR light (Table 1, entries 12, 13), which is more favor for the utilization of solar energy. Furthermore, a lower pressure leads to a lower CO_2 conversion and C_{2+} selectivity (Table S4, Supporting Information).

The experimental results presented illustrate nicely that the surface chemical composition of the CoFe-*x* catalysts, and correspondingly the CO_2 hydrogenation activity and product selectivity, can be favorably manipulated simply by changing the reduction temperature of CoFeAl-LDH nanosheets precursor. For CoFe-*x*, the product selectivity progressively shifted from exclusively CO at 300–400 °C, to CH_4 at 450–550 °C, and finally more valuable hydrocarbons compounds at precursor reduction temperatures ≥600 °C. The catalyst synthesis strategy introduced in this work, involving H_2 reduction of compositionally flexible LDH nanosheets, is so simple and low cost that it is likely to be widely adopted for the development of solar-driven photothermal catalysts for other challenging chemical transformations.

Due to the excellent performance of the CoFe-*x* catalysts, especially those prepared by H_2 reduction at temperatures ≥ 600 °C, a detailed study of the structural evolution of the

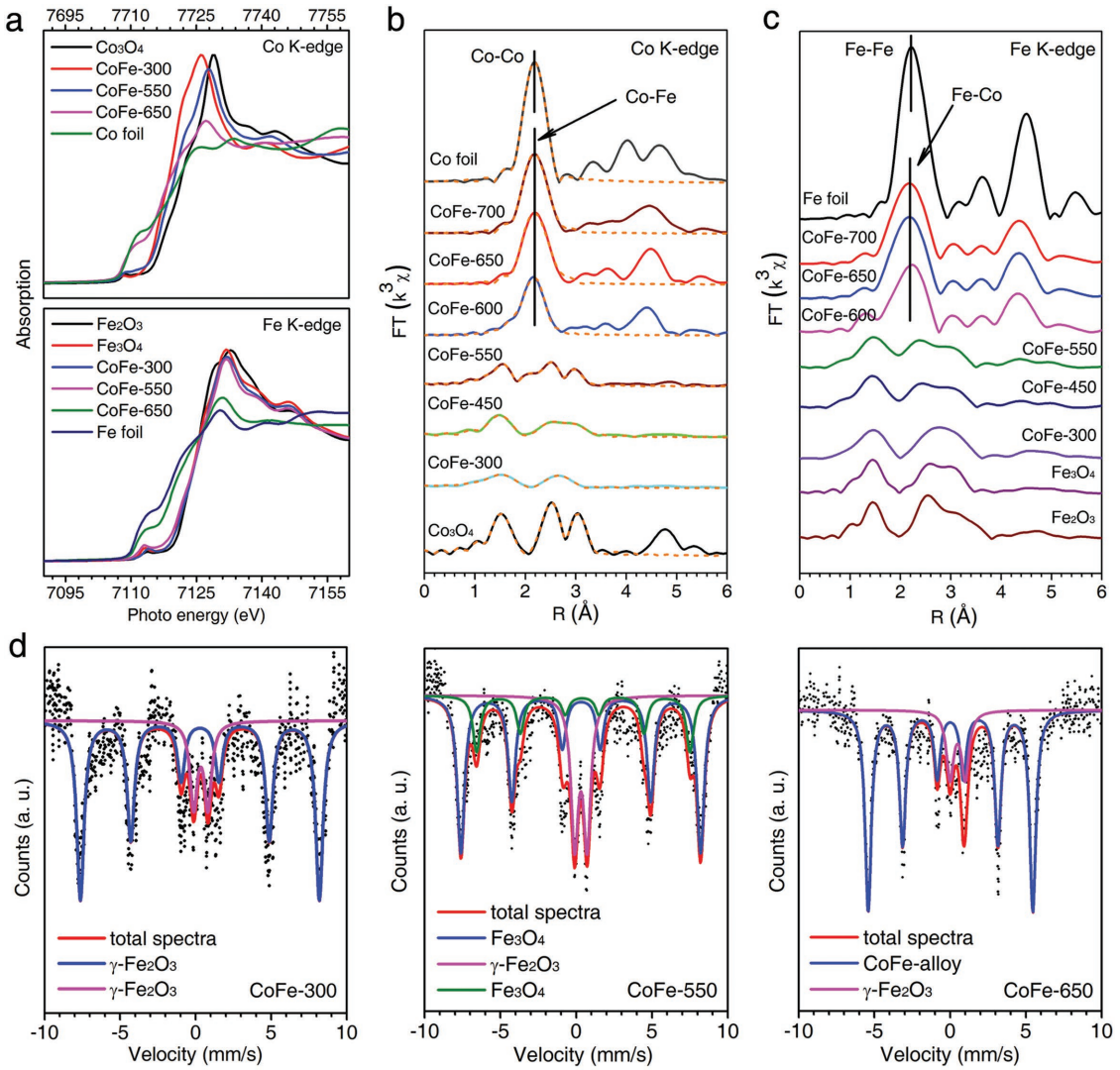

Figure 2. a–c) Co K-edge and Fe K-edge XANES spectra (a) and corresponding Fourier transforms of the k^3 weighted EXAFS spectra at the Co K-edge (b) and Fe K-edge (c) for different CoFe-*x* samples. d) Mössbauer spectra for CoFe-300, CoFe-550, and CoFe-650. The solid lines show the curve fits to the raw data. Average uncertainties in Mössbauer parameters: ±0.03, Fe fraction; ±5 kG, hyperfine magnetic field; ±0.03 mm s^{-1}, isomer shift; ±0.05 mm s^{-1}, quadrupole splitting.

CoFe-*x* catalysts with reduction temperature was undertaken using X-ray absorption near-edge structure (XANES) and extended X-ray absorption fine structure (EXAFS). Co K-edge and Fe K-edge XANES spectra (**Figure 2**a) show that as the CoFeAl-LDH nanosheets reduction temperature was increased from 300 to 650 °C, both Co and Fe in the CoFe-*x* catalysts were transformed from cationic states to metallic form. CoFe-650 showed the conspicuous absorption edge features typical for Co^0 and Fe^0. Corresponding EXAFS spectra for CoFe-650 and other CoFe-*x* catalysts reduced at or above 600 °C (Figure 2b,c; Table S5, Supporting Information) revealed the formation of new Co—Fe bonds, consistent with CoFe alloy nanoparticle formation previously confirmed by XRD.

The Mössbauer spectroscopy technique is a powerful tool for quantifying the oxidations states of iron in complex samples, and was successfully applied here for quantification of Fe species in the CoFe-*x* catalysts. Mössbauer spectra

Table 2. Mössbauer parameters for selected CoFe-*x* collected at room temperature.

Catalysts	Percent [%]	IS[a] [mm s^{-1}]	QS[b] [mm s^{-1}]	*T*	Line width	Fe states
CoFe-300	80.9	0.29	−0.01	49.15	0.58	γ-Fe_2O_3
	19.1	0.34	0.94	–	0.58	γ-Fe_2O_3
CoFe-550	55.1	0.32	−0.03	49.16	0.58	Fe_3O_4
	19.8	0.43	0.08	43.74	0.58	Fe_3O_4
	25.1	0.31	0.82	–	0.58	γ-Fe_2O_3
CoFe-650	83.5	0.02	0.02	33.70	0.49	CoFe-alloy
	16.5	0.49	1.00	–	0.58	γ-Fe_2O_3

[a]IS, isomer shift, relative to α-Fe at room temperature; [b]QS, electric quadrupole splitting.

for selected CoFe-*x* catalysts are shown in Figure 2d, with the hyperfine interaction parameters summarized in **Table 2**. For CoFe-300, the sextet with ^{57}Fe Mössbauer parameters of IS = 0.29 mm s^{-1} and QS = –0.01 mm s^{-1} accounted for about 80.9% of Fe present in the sample, and can be readily assigned to octahedrally coordinated Fe^{3+} in γ-Fe_2O_3. The weaker doublet (19.1% of total Fe) is assigned to γ-Fe_2O_3 with a smaller particle size.[17] On increasing the CoFeAl-LDH nanosheets reduction temperate to 550 °C, some of the γ-Fe_2O_3 was reduced to Fe_3O_4. The Mössbauer spectrum of CoFe-550 could be fitted by three sextets (one for γ-Fe_2O_3 and two for Fe_3O_4). For the Fe_3O_4 component, the sextet with IS = 0.32 mm s^{-1} and QS = –0.03 mm s^{-1} can be associated to the tetrahedral Fe^{3+} ions, whist that with IS = 0.43 mm s^{-1} and QS = 0.08 mm s^{-1} can be assigned to the octahedral Fe^{3+} + Fe^{2+} ions of the inverse spinel structure of Fe_3O_4.[4d,18] Mössbauer analysis of CoFe-650 confirmed CoFe-alloy formation.[19] Small amounts of γ-Fe_2O_3 were found in both CoFe-550 (25.1%) and CoFe-650 (16.5%) due to the partially oxidation of Fe-containing species exposed in air.

Since the CoFe-*x* catalysts were derived from a CoFeAl-LDH nanosheet precursor, the stepwise evolution of nanosheets morphology at different reduction temperatures was of particular interest regarding the possible active sites for CO_2 hydrogenation, and studied in detail by transmission electron microscopy (TEM). For CoFe-300 (Figure S9, Supporting Information), Fe_2O_3 nanoparticles appeared, uniformly dispersed on a CoAl-mixed metal oxide nanosheet support. For CoFe-550 (Figure S10, Supporting Information), both CoO_x and FeO_x were identified on a nanosheet support (presumably amorphous alumina). For CoFe-650, dense nanoparticles with a diameter of ≈30 nm decorated the nanosheet support (**Figure 3**). The nanoparticles showed a homogeneous distribution of Co and Fe (Co:Fe = 2:1, atomic ratio, Figure S11, Supporting Information), whilst the support contained Al and O suggesting it was composed of an amorphous Al_2O_3[15] (Figure 3d; Figure S12, Supporting Information). An energy dispersive spectroscopy (EDS) line over several of the 30 nm nanoparticles provided further evidence for a homogeneous distribution of Co and Fe in the nanoparticles (Figure 3e). Lattice fringes with a spacing of 0.201 nm were found by high-resolution TEM (HRTEM) analysis on the nanoparticles, corresponding to the (110) plane of bcc CoFe alloy. The identification of discrete CoFe alloy nanoparticles by TEM and HRTEM for CoFe-650 is consistent with the findings of XRD, XAFS, and Mössbauer spectroscopy analyses. In conjunction with the CO_2 hydrogenation data in Figure 1, it becomes immediately apparent that the formation of these CoFe alloy nanoparticles was key to the strong photothermal response of CoFe-650 and thus its excellent performance for CO_2 hydrogenation with high selectivity to C_{2+} hydrocarbons. Comparative experiments using catalysts prepared from LDH precursors with different Co:Fe atom ratios (1:1, 2:1, and 3:1) revealed that the 2:1 ratio yielded the best photothermal catalytic performance (Figures S13–S15 and Table S6, Supporting Information). In order to confirm the active role of bimetallic CoFe alloy nanoparticles in the CO_2 hydrogenation reaction, single metal Co or Fe-based metal catalysts were synthesized by H_2-reduction of CoAl-LDH and MgFeAl-LDH nanosheets precursors at 650 °C, respectively (Figures S16 and S17, Supporting Information), and their performance for CO_2 hydrogenation under UV–vis excitation evaluated. The corresponding Co-650 and Fe-650 catalysts (supported by alumina nanosheets and alumina–magnesia nanosheets, respectively) showed very high CH_4 and CO selectivities, respectively (Table S7, Supporting Information). The data confirm that the CoFe alloy nanoparticles in the CoFe-650 catalyst are responsible for the formation of valuable C_{2+} hydrocarbons during CO_2 hydrogenation under UV–vis excitation.

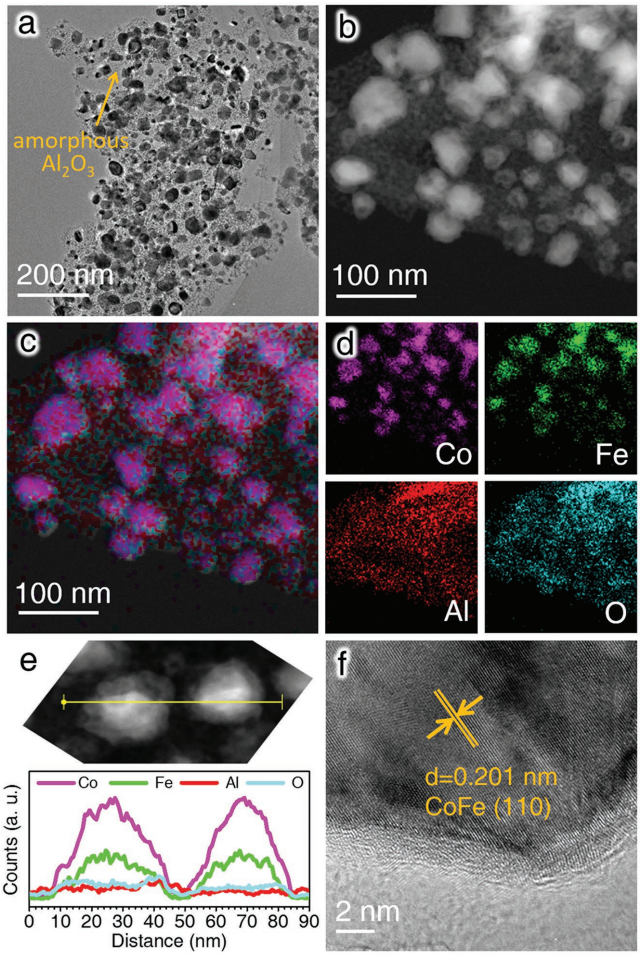

Figure 3. Characterization data for CoFe-650. a) TEM image. b) High-angle annular dark-field scanning TEM (HAADF-STEM) image. c,d) Overlayed EDS element map (c) and individual EDS maps for Co, Fe, Al, and O (d). e) EDS line-scan element profile over two adjacent nanoparticles. f) HRTEM image confirming formation of a discrete CoFe alloy nanoparticle.

DFT calculations were further performed in order to better understand the excellent catalytic properties of Co–Fe alloy nanoparticles. Based on our experimental characterization results, the following catalyst models were constructed to represent the different CO_2 reduction catalyst prepared in this study from LDH nanosheets precursor: Fe_2O_3 (110), Fe_3O_4 (110), Co_3O_4 (100) to represent CoFe-300 and CoFe-550; $Co_{11}Fe_5$ (110) to represent CoFe-650; Co(10-11) and Fe(110) to represent Co-650 and Fe-650, respectively (Figures S18 and S19, Supporting Information). It is generally considered that the formation of value-added compounds from CO_2 hydrogenation (via a non-methanol-mediated process) proceeds two steps: RWGS reaction and FT synthesis.[4b]

Thus, it is highly necessary to study the CO-intermediate adsorption behavior and its C—C coupling ability over the catalysts. For the Fe_2O_3 (110), Fe_3O_4 (110), and Co_3O_4 (100) surfaces, the adsorption energies to CO were very similar (–0.72, –0.84, and –0.92 eV, respectively, Figure S20, Supporting Information). Therefore, in order to understand the different catalytic properties of CoFe-300 and CoFe-550, the hydrogenation of CO on the Fe_2O_3 (110), Fe_3O_4 (110), and Co_3O_4 (100) surfaces needed to be considered (**Figure 4**a). Calculations of CO hydrogenation into CHO on Fe_2O_3 (110) and Fe_3O_4 (110) gave reaction energies of 2.57 and 1.19 eV, indicating that these processes are difficult thermodynamically when compared with CO desorption. For the Co_3O_4 (100) surface, all the four steps of CO hydrogenation into CH_4 are favorable thermodynamically, with the total reaction energy being exothermic by 0.91 eV. These calculations thus readily explain why Fe-based catalysts (e.g., CoFe-300, Fe_2O_3, and Fe_3O_4) favor the production of CO during CO_2 hydrogenation, whereas Co-based or Co-rich catalysts (CoFe-550 and Co_3O_4) favor the production of CH_4 during CO_2 hydrogenation.

For hydrocarbon formation by the catalytic CO_2 hydrogenation, the most possible C—C coupling path (to CH—CH_2) is computed on the $Co_{11}Fe_5$ (110), Co (10-11), and Fe (110) surfaces (Figure 4b). The calculation results show that the barrier to adsorbed CH—CH_2 on the $Co_{11}Fe_5$ (110) surface was 0.86 eV, lower than the corresponding barriers on the Co (10-11) and Fe (110) surfaces (1.05 and 1.10 eV, respectively). The calculations provide strong evidence to support the experimentally derived hypothesis that CoFe bimetallic alloy catalysts (i.e., CoFe-650) promote C—C coupling reactions during CO_2 hydrogenation.

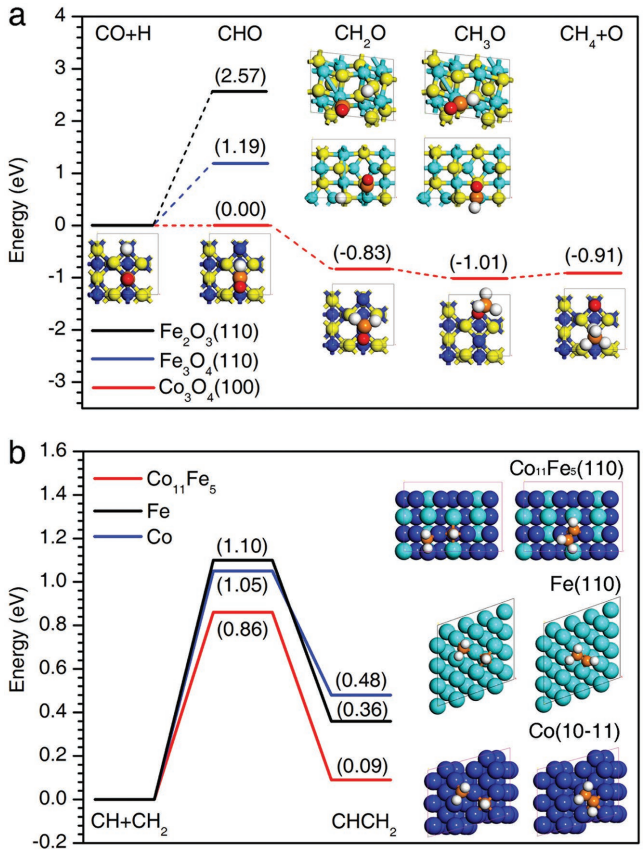

Figure 4. a) The reaction path for CO hydrogenation on Fe_2O_3 (110), Fe_3O_4 (110), and Co_3O_4 (100) surfaces. Co, Fe, C, O, and H atoms are represented by blue, cyan, orange, yellow, and white spheres, respectively; in order to distinguish the O atom in CO, it is shown in red. b) Probable C—C coupling path (to CH—CH_2) on $Co_{11}Fe_5$ (110), Co (10–11), and Fe (110). In the surface models, Co, Fe, C, and H atoms are represented by blue, cyan, orange, and white spheres, respectively.

Based on the experimental and computational results presented herein, a close structure-activity relationship was established for CO_2 hydrogenation over CoFe-*x* catalysts under UV–vis excitation. When the CoFeAl-LDH nanosheet reduction temperature reached 300 °C, the Fe species migrated to the surface of the collapsed nanosheets to form FeO_x nanoparticles. The FeO_x nanoparticles served as catalytic active species to promote the CO_2 hydrogenation to CO. The activity of FeO_x for the generation of CO during CO_2 hydrogenation was confirmed in control experiments (Table 1, entries 14, 15) and supported by DFT calculations. At precursor reduction temperatures between 450 and 550 °C, the Co species then migrated out to the surface of the nanosheets to form FeO_x/CoO_x nanoparticles (supported by amorphous Al_2O_3 nanosheets). The FeO_x/CoO_x nanoparticles were active for CO_2 hydrogenation, with the CoO_x domains giving high selectivity to CH_4 and the FeO_x domains favoring CO production. Methane was the dominant product formed, consistent with control tests conducted using Co_3O_4 and a mixture of Co_3O_4 and Fe_3O_4 (Table 1, entries 16, 17). García and co-workers reported that the photocatalytic hydrogenation of CO_2 over CoO_x and FeO_x yielded CH_4 and CO, respectively, suggesting that CO_2 hydrogenation over the CoFe-300 and CoFe-550 catalysts under UV–vis irradiation may also utilize a photocatalytic reaction pathway.[20] At reduction temperatures above 600 °C, the alumina-supported FeO_x/CoO_x were reduced to form alumina-supported CoFe-alloy nanoparticles, which possessed high CO_2 hydrogenation activity and product selectivities to hydrocarbons resulting from the unique electronic and light absorption properties of the CoFe alloy nanoparticles that allowed exploitation of photothermal effects. The synthesis of the different CoFe-*x* catalysts and their catalytic activity toward CO_2 hydrogenation under simulated solar excitation can be summarized in Scheme 1.

In conclusion, a series of CoFe-based catalysts were successfully fabricated by H_2-reduction of a CoFeAl-LDH nanosheet precursor at 300–700 °C. By controlling the reduction temperature (*x*), three distinct CoFe-*x* catalysts were obtained that showed markedly different activity and product selectivities in CO_2 hydrogenation under UV–vis excitation. At precursor reduction temperatures above 600 °C, alumina-supported CoFe alloy catalysts were obtained, which demonstrated high CO_2 conversions and remarkable selectivity (≈95%) toward hydrocarbons (>35% selectivity to C_{2+} hydrocarbons) by a photothermal effect. DFT calculations confirmed the key role of the CoFe alloy structure in promoting C—C coupling reactions during CO_2 hydrogenation. This work demonstrates a completely new approach for harnessing abundant solar-energy to produce high-value hydrocarbons from a CO_2 feedstock.

Supporting Information

Supporting Information is available from the Wiley Online Library or from the author.

Acknowledgements

G.C., R.G., and Y.Z. contributed equally to this work. The authors are grateful for the financial support from the National Key Projects for Fundamental Research and Development of China (2016YFB0600901, 2017YFA0206904, and 2017YFA0206900), the Ministry of Science and Technology of China (2014CB239402 and 2013CB834505), the National Natural Science Foundation of China (51772305, 51572270, U1662118, 21401206, 21401207, 91545121, and 21473229), the Strategic Priority Research Program of the Chinese Academy of Sciences (XDB17000000), the Young Elite Scientist Sponsorship Program by CAST (YESS), and the Youth Innovation Promotion Association of the CAS. The XAFS experiments were conducted in 1W1B beamline of Beijing Synchrotron Radiation Facility (BSRF).

Conflict of Interest

The authors declare no conflict of interest.

Keywords

CoFe alloy, layered double hydroxides, photothermal CO_2 hydrogenation, solar-to-fuel conversion, value-added compounds

Received: August 16, 2017
Revised: September 27, 2017
Published online: December 5, 2017

[1] a) T. P. Hughes, A. H. Baird, D. R. Bellwood, M. Card, S. R. Connolly, C. Folke, R. Grosberg, O. Hoegh-Guldberg, J. B. C. Jackson, J. Kleypas, J. M. Lough, P. Marshall, M. Nyström, S. R. Palumbi, J. M. Pandolfi, B. Rosen, J. Roughgarden, *Science* **2003**, *301*, 929; b) J. A. Patz, D. Campbell-Lendrum, T. Holloway, J. A. Foley, *Nature* **2005**, *438*, 310.

[2] a) D. M. D'Alessandro, B. Smit, J. R. Long, *Angew. Chem., Int. Ed.* **2010**, *49*, 6058; b) V. Scott, S. Gilfillan, N. Markusson, H. Chalmers, R. S. Haszeldine, *Nat. Clim. Change* **2013**, *3*, 105; c) Q. Yi, W. Li, J. Feng, K. Xie, *Chem. Soc. Rev.* **2015**, *44*, 5409.

[3] a) S. Lin, C. S. Diercks, Y.-B. Zhang, N. Kornienko, E. M. Nichols, Y. Zhao, A. R. Paris, D. Kim, P. Yang, O. M. Yaghi, C. J. Chang, *Science* **2015**, *349*, 1208; b) S. Gao, Y. Lin, X. Jiao, Y. Sun, Q. Luo, W. Zhang, D. Li, J. Yang, Y. Xie, *Nature* **2016**, *529*, 68; c) Y. Ma, X. Wang, Y. Jia, X. Chen, H. Han, C. Li, *Chem. Rev.* **2014**, *114*, 9987; d) C. Gao, Q. Meng, K. Zhao, H. Yin, D. Wang, J. Guo, S. Zhao, L. Chang, M. He, Q. Li, H. Zhao, X. Huang, Y. Gao, Z. Tang, *Adv. Mater.* **2016**, *28*, 6485; e) R. D. Richardson, E. J. Holland, B. K. Carpenter, *Nat. Chem.* **2011**, *3*, 301; f) B. Chatelet, L. Joucla, J.-P. Dutasta, A. Martinez, K. C. Szeto, V. Dufaud, *J. Am. Chem. Soc.* **2013**, *135*, 5348; g) H. Seo, M. H. Katcher, T. F. Jamison, *Nat. Chem.* **2016**, *9*, 453; h) Q. Liu, L. Wu, R. Jackstell, M. Beller, *Nat. Commun.* **2015**, *6*, 5933.

[4] a) R. W. Dorner, D. R. Hardy, F. W. Williams, H. D. Willauer, *Energy Environ. Sci.* **2010**, *3*, 884; b) W. Wang, S. Wang, X. Ma, J. Gong, *Chem. Soc. Rev.* **2011**, *40*, 3703; c) S. Saeidi, N. A. S. Amin, M. R. Rahimpour, *J. CO2 Util.* **2014**, *5*, 66; d) J. Wei, Q. Ge, R. Yao, Z. Wen, C. Fang, L. Guo, H. Xu, J. Sun, *Nat. Commun.* **2017**, *8*, 15174.

[5] a) H. Muroyama, Y. Tsuda, T. Asakoshi, H. Masitah, T. Okanishi, T. Matsui, K. Eguchi, *J. Catal.* **2016**, *343*, 178; b) P. Frontera, A. Macario, M. Ferraro, P. Antonucci, *Catalysts* **2017**, *7*, 59; c) K. Jalama, *Cat. Rev.* **2017**, *59*, 95.

[6] a) A. N. Akin, M. Ataman, A. E. Aksoylu, Z. I. Önsan, *React. Kinet. Catal. Lett.* **2002**, *76*, 265; b) C. G. Visconti, M. Martinelli, L. Falbo, L. Fratalocchi, L. Lietti, *Catal. Today* **2016**, *277*, 161; c) G. Centi, E. A. Quadrelli, S. Perathoner, *Energy Environ. Sci.* **2013**, *6*, 1711.

[7] a) M. K. Gnanamani, G. Jacobs, H. H. Hamdeh, W. D. Shafer, B. H. Davis, *Catal. Today* **2013**, *207*, 50; b) U. Rodemerck, M. Holeňa, E. Wagner, Q. Smejkal, A. Barkschat, M. Baerns, *ChemCatChem* **2013**, *5*, 1948; c) P. Gao, S. Li, X. Bu, S. Dang, Z. Liu, H. Wang, L. Zhong, M. Qiu, C. Yang, J. Cai, W. Wei, Y. Sun, *Nat. Chem.* **2017**, *9*, 1019.

[8] M. D. Porosoff, B. Yan, J. G. Chen, *Energy Environ. Sci.* **2016**, *9*, 62.

[9] G. A. Olah, G. K. S. Prakash, A. Goeppert, *J. Am. Chem. Soc.* **2011**, *133*, 12881.

[10] X. Meng, T. Wang, L. Liu, S. Ouyang, P. Li, H. Hu, T. Kako, H. Iwai, A. Tanaka, J. Ye, *Angew. Chem., Int. Ed.* **2014**, *53*, 11478.

[11] a) H. Zhang, T. Wang, J. Wang, H. Liu, T. D. Dao, M. Li, G. Liu, X. Meng, K. Chang, L. Shi, T. Nagao, J. Ye, *Adv. Mater.* **2016**, *28*, 3703; b) J. Ren, S. Ouyang, H. Xu, X. Meng, T. Wang, D. Wang, J. Ye, *Adv. Energy Mater.* **2016**, *7*, 1601657.

[12] a) C. Wang, O. Ranasingha, S. Natesakhawat, P. R. Ohodnicki, M. Andio, J. P. Lewis, C. Matranga, *Nanoscale* **2013**, *5*, 6968; b) P. G. O'Brien, A. Sandhel, T. E. Wood, A. A. Jelle, L. B. Hoch, D. D. Perovic, C. A. Mims, G. A. Ozin, *Adv. Sci.* **2014**, *1*, 1400001; c) J. Jia, P. G. O'Brien, L. He, Q. Qiao, T. Fei, L. M. Reyes, T. E. Burrow, Y. Dong, K. Liao, M. Varela, S. J. Pennycook, M. Hmadeh, A. S. Helmy, N. P. Kherani, D. D. Perovic, G. A. Ozin, *Adv. Sci.* **2016**, *3*, 1600189; d) W. Zhang, L. Wang, K. Wang, M. U. Khan, M. Wang, H. Li, J. Zeng, *Small* **2017**, *13*, 1602583; e) X. Zhang, X. Li, D. Zhang, N. Q. Su, W. Yang, H. O. Everitt, J. Liu, *Nat. Commun.* **2017**, *8*, 14542.

[13] a) M. Claeys, M. E. Dry, E. van Steen, P. J. van Berge, S. Booyens, R. Crous, P. van Helden, J. Labuschagne, D. J. Moodley, A. M. Saib, *ACS Catal.* **2015**, *5*, 841; b) X. Peng, K. Cheng, J. Kang, B. Gu, X. Yu, Q. Zhang, Y. Wang, *Angew. Chem., Int. Ed.* **2015**, *54*, 4553; c) N. E. Tsakoumis, J. C. Walmsley, M. Rønning, W. van Beek, E. Rytter, A. Holmen, *J. Am. Chem. Soc.* **2017**, *139*, 3706; d) V. Navarro, M. A. van Spronsen, J. W. M. Frenken, *Nat. Chem.* **2016**, *8*, 929.

[14] a) Q. Wang, D. O'Hare, *Chem. Rev.* **2012**, *112*, 4124; b) M.-Q. Zhao, Q. Zhang, W. Zhang, J.-Q. Huang, Y. Zhang, D. S. Su, F. Wei, *J. Am. Chem. Soc.* **2010**, *132*, 14739; c) G. Fan, F. Li, D. G. Evans, X. Duan, *Chem. Soc. Rev.* **2014**, *43*, 7040; d) X. Zhao, F. Zhang, S. Xu, D. G. Evans, X. Duan, *Chem. Mater.* **2010**, *22*, 3933; e) S. He, C. Li, H. Chen, D. Su, B. Zhang, X. Cao, B. Wang, M. Wei, D. G. Evans, X. Duan, *Chem. Mater.* **2013**, *25*, 1040; f) W. Gao, Y. Zhao, H. Chen, H. Chen, Y. Li, S. He, Y. Zhang, M. Wei, D. G. Evans, X. Duan, *Green Chem.* **2015**, *17*, 1525.

[15] Y. Zhao, B. Zhao, J. Liu, G. Chen, R. Gao, S. Yao, M. Li, Q. Zhang, L. Gu, J. Xie, X. Wen, L.-Z. Wu, C.-H. Tung, D. Ma, T. Zhang, *Angew. Chem., Int. Ed.* **2016**, *55*, 4215.

[16] a) E. Y. Lukianova-Hleb, A. N. Volkov, X. Wu, D. O. Lapotko, *Adv. Mater.* **2013**, *25*, 772; b) Q. Chen, L. Xu, C. Liang, C. Wang, R. Peng, Z. Liu, *Nat. Commun.* **2016**, *7*, 13193; c) Q. Yang, Q. Xu, S.-H. Yu, H.-L. Jiang, *Angew. Chem., Int. Ed.* **2016**, *55*, 3685.

[17] Z. Xiao, S. Jin, X. Wang, W. Li, J. Wang, C. Liang, *J. Mater. Chem.* **2012**, *22*, 16598.

[18] H. Zhou, J. Yin, Z. Nie, Z. Yang, D. Li, J. Wang, X. Liu, C. Jin, X. Zhang, T. Ma, *J. Mater. Chem. A* **2016**, *4*, 67.

[19] a) T. Szumiata, M. Gzik-Szumiata, K. Brzózka, B. Górka, M. Gawroński, A. Caruana Finkel, N. Reeves-McLaren, N. A. Morley, *J. Magn. Magn. Mater.* **2016**, *401*, 943; b) M. K. Gnanamani, G. Jacobs, H. H. Hamdeh, W. D. Shafer, F. Liu, S. D. Hopps, G. A. Thomas, B. H. Davis, *ACS Catal.* **2016**, *6*, 913.

[20] F. Sastre, A. V. Puga, L. Liu, A. Corma, H. García, *J. Am. Chem. Soc.* **2014**, *136*, 6798.